LOCATION OF CURVED EDGES TO SUBPIXEL VALUES

Ling-Hwei Chen and Wen-Hsiang Tsai*

Department of Computer and Information Science
National Chiao Tung University
Hsinchu, Taiwan 30050, R.O.C.

Key Words: curved edge detection, line-type edge detection, moment-preserving, parabolic equation, subpixel accuracy.

ABSTRACT

The problem of detecting step edge points which fall on curves (called curved edge points) is solved. Based on the moment-preserving principle, the solution can be used to estimate curved edge locations to subpixel accuracy. The locations are approximated by parabolic equations. Experimental results, which show that the proposed detector is more effective for detecting curved edges and boundary corners than conventional line-type edge detectors, are included.

一偵測曲線邊緣至次像素準確度之方法

陳玲慧　蔡文祥*

國立交通大學資訊科學研究所

摘　要

本論文主要提出一偵測曲線邊緣之方法。基於矩量不變原理，本方法可用來估計曲線邊緣位置至次像素準確度。而曲線邊緣位置是利用拋物線來逼近。實驗結果顯示，本方法用來評估曲線邊緣比一般用線來逼近的方法有效。

INTRODUCTION

Edge detection plays an important role in image processing. Many edge detectors with ''pixel'' accuracy have been developed. For a survey of these techniques, see [11]. The gradient and the Laplacian operators are two basic edge detectors for noiseless pictures. They are difference operators that respond to changes in gray levels [11]. To reduce the effect of noise on the response of a difference operator, some operators that compute differences of local averages were proposed [3,11]. In addition, many approaches to modifying the gradient and the Laplacian operators have also been provided. Frei and Chen [4] developed a set of orthogonal functions which were closely related to distinct image features and allowed efficient extraction of object boundary elements. Schachter and Rosenfeld [12] also provided three operators for edge detection. The first used the maximum of the x and y second-order differences. The second used the difference between the mean and the median gray levels in a neighborhood. The third used the distance between the center and the centroid of a neighborhood as an edge value.

Jacobus and Chien [10] introduced two edge detection algorithms, one difference-based and the other adaptive-threshold-based. With these operators, edge positions may be computed to greater precision than the basic pixel size. Shipman et al. [13] presented a diffuse edge detection and a fitting procedure. In the approach, a straight line is used to estimate edge locations. The

*Correspondence addressee

line may be fitted by choosing its direction as normal to the weighted average gradient direction in a square domain and passing through the weighted center of mass of the gradient points.

Suk and Hong [14] described an edge extraction technique specifically developed for noisy images which eliminated the necessity of noise removal preprocessing or postprocessing. The algorithm was based on parallel statistical tests for which indeterminate decisions were allowed. Haralick [6] defined an edge to occur at a pixel if and only if there exists a certain point in the pixel area having a negatively-sloped zero crossing of the second directional derivative taken in the direction of a nonzero gradient at the pixel center. To determine whether or not a pixel is a step edge pixel, a linear function of tensor products of discrete orthogonal polynomials of up to degree three was used to estimate the underlying gray tone intensity surface. Then, the appropriate directional derivatives were easily computed from the function.

In the real world, the gray value of a step edge point always lies between those of the two neighboring regions, each with nearly constant gray values. Based on this fact and the moment-preserving principle, Chen and Wang [2] presented a deterministic method to locate all of the edge points.

Some problems, such as calibration, remotely-sensed imagery edge detection, image-to-image and image-to-map registration, etc., need accurate measurement. To solve such problems, several investigators have tried to develop methods to get edge locations with "subpixel" accuracy. Hueckel [8] first presented a local edge detector of this type for two-dimensional images. The operator used a line equation to approximate a given empirical edge in a disk neighborhood of a point, so that the measure of the square of the Hilbert distance of the gray values between the input data and the output data was minimized. The line equation can then be used to calculate the edge location to subpixel accuracy. Hartley [7] presented a Hueckel-like edge detector in which Hueckel's weighting function over a bounded disk was replaced by the Gaussian function over the entire plane. The edge detector is a generalization of both the Gaussian-weighted gradient edge detector and the zero-crossing edge detector.

By preserving the first three gray moment function values in a pixel neighborhood, Tabatabai and Mitchell [16] presented a subpixel edge detector, which also derived a line equation to calculate a local edge location. By the assumption that the edges are locally straight, Hyde and Davis [9] provided another subpixel line edge detector which best predicts the intensities of the pixels along the edge.

The above methods all have a common disadvantage, i.e., they used line equations to approximate edge locations. This is not appropriate when the edge is curved or there exist corners in the detection area. In this paper, a method is proposed to estimate curved step edge locations locally using a parabolic equation. The method is also based on the moment-preserving principle, and curved edge points can be detected to subpixel accuracy. Since a line equation is a degeneration case of a parabolic equation, the method works as well as the Tabatabai-Mitchell's detector for line-type edges.

In the remainder of this paper, we first describe the curved edge operator. The parabolic equation is then derived and the equation coefficients solved. Finally, some experimental results are presented to show the superiority of the proposed method over conventional line-type edge detectors in the capability of curved edge detection.

PROPOSED CURVED EDGE DETECTOR

The proposed curved edge detector approximates a step edge location by a parabolic equation with three parameters which will be calculated according to certain criteria as discussed in the following sections. Similar to the Tabatabai-Mitchell edge detector, the proposed detector accepts as input a set of 69 pixels arranged in such a way to best approximate the area of a cricle with 4.5 units in radius (see Fig. 1a for an illustration). The detector generates as output a parabolic equation as well as two intensity values h_1 and h_2 (assume $h_2 > h_1$). The parabola separates the circle into two regions A_1 and A_2

		251	248	245	2	9		
	255	248	247	254	5	7	2	
251	255	253	254	253	3	8	1	3
245	252	249	246	249	7	9	6	1
254	251	245	252	249	3	3	2	2
3	1	4	5	5	1	8	7	3
6	1	7	0	9	9	5	1	1
	5	9	7	9	10	6	6	
		5	4	7	5	10		

(a) Input data in a 4.5-unit circle.

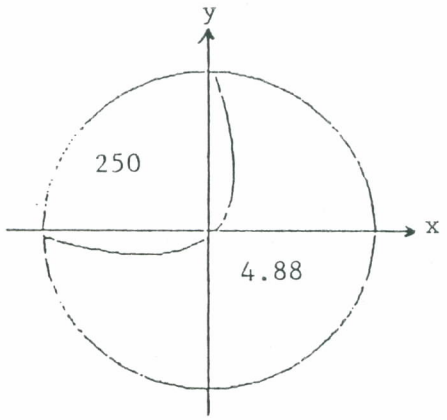

(b) Output data with $h_1 = 4.88$ and $h_2 = 250$.

Fig. 1. Curved edge detection on a 4.5-unit circle.

with h_1 and h_2 as the representative intensity values for A_1 and A_2, respectively, as is illustrated in Fig. 1b.

In this approach, we assume that the symmetrical axis of the parabola passes the center of the circle and the axis direction is defined to be toward the A_2 area (see Fig. 2a). This is reasonable because the circle size is small. Note that if the symmetrical axis does not pass through the center of the circle, a certain technique has been proposed to solve the problem, which will be discussed later in Section V. If the angle between the symmetrical axis and the X-axis is q, we can rotate the circle counterclockwise with respect to the origin through an angle of $\pi/2$-q so that the symmetrical axis of the rotated parabola coincides with the Y-axis (see Fig. 2b). Then, the new coordinates (x', y') of the rotated parabola can be expressed by the coordinates (x,y) of the original parabola as

$$x' = xsinq - ycosq$$

$$y' = xcosq + ysinq \ , \qquad (1)$$

and the equation for the rotated parabola can be expressed as

$$y' = ax'^2 + b \ . \qquad (2)$$

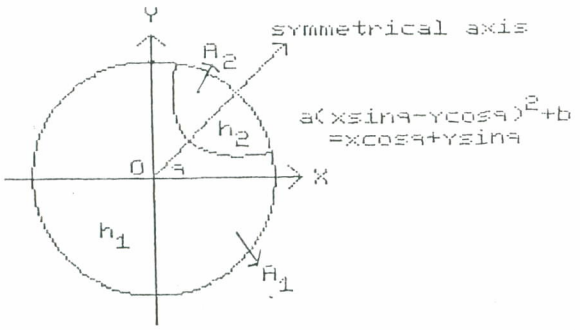

(a) Parabolic edge equation as a function of q, a, and b.

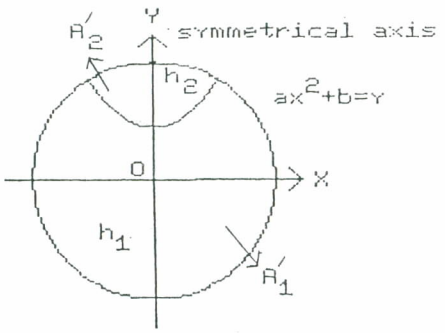

(b) Parabolic edge equation as a function of a and b after rotating counterclockwise with respect to the origin through an angle of $\pi/2-q$.

Fig. 2. The parabola before and after rotation.

Combining (1) and (2), we get the original parabolic equation as

$$a(xsinq - ycosq)^2 + b = xcosq + ysinq \ . \qquad (3)$$

Hence, the three parameters a, b, and q determine the parabola. In the next two sections, we will derive some equations for computing a, b, and q.

DERIVATIONS OF THE EQUATIONS FOR COMPUTING THE q PARAMETER

In this section, we prove several theorems which lead to the equations for computing the q parameter. Assume that the curved edge operator has been applied to a 4.5-unit circle, resulting in a parabola described by Eq. (3), which separates the circle into two regions, A_1 and A_2, with intensity values h_1 and h_2, respectively. Define

$$\bar{x} = \frac{h_1 \int_{A_1}\int xdxdy + h_2 \int_{A_2}\int xdxdy}{h_1 \int_{A_1}\int dxdy + h_2 \int_{A_2}\int dxdy} \ , \qquad (4)$$

$$\bar{y} = \frac{h_1 \int_{A_1}\int ydxdy + h_2 \int_{A_2}\int ydxdy}{h_1 \int_{A_1}\int dxdy + h_2 \int_{A_2}\int dxdy} \ , \qquad (5)$$

as the coordinates of the center of gravity of the intensities of the output data inside the circle [16].

If we rotate the circle counterclockwise with respect to the origin through an angle of $\pi/2$-q (see Fig. 2), then the symmetrical axis of the rotated parabola will coincide with the Y-axis. Let $(\bar{x}', \bar{y}')$ be the coordinates of the center of gravity of the intensities inside the rotated circle, in which the rotated parabola separates the circle into two regions, A_1' and A_2' (see Fig. 2b). Then it can be shown [15] that $(\bar{x}', \bar{y}')$ are related to $(\bar{x},\bar{y})$ through (1). Furthermore, we have the following theorem.

THEOREM 1 $\bar{x}' = 0, \bar{y}' > 0$.

Proof Since the rotated parabola is symmetric to the Y-axis, it is easily seen that $\bar{x}' = 0$. To show that $\bar{y}' > 0$, we see first that the rotated parabola intersects the circle in twelve distinct ways as shown in Fig. 3. Next, we redraw Fig. 3 as shown in Fig. 4.

In Fig. 4, we have divided each circle into three or four parts B, D, C_b, and C_d. A_1' is composed of B and C_b, and A_2' is composed of D and C_d. It follows that

$$\bar{y}' = \frac{h_1 \int_{A_1'}\int y'dx'dy' + h_2 \int_{A_2'}\int y'dx'dy'}{h_1 \int_{A_1'}\int dx'dy' + h_2 \int_{A_2'}\int dx'dy'} \qquad (6)$$

$$= \frac{h_1 \left(\int_B\int y'dx'dy' + \int_{C_b}\int y'dx'dy'\right)}{h_1 \int_{A_1'}\int dx'dy' + h_2 \int_{A_2'}\int dx'dy'}$$

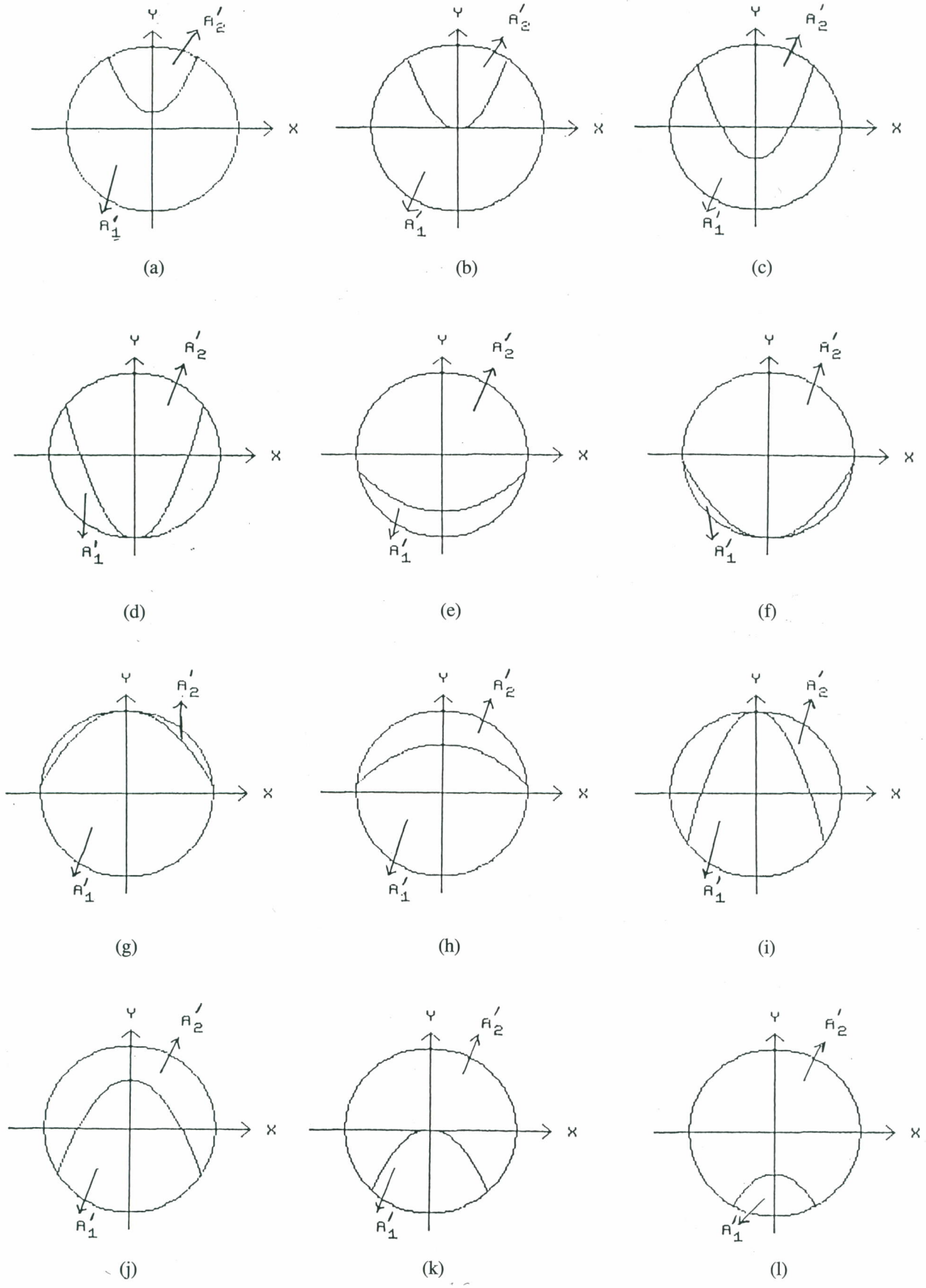

Fig. 3. The rotated parabola intersects the 4.5-unit circle in twelve distinct ways.

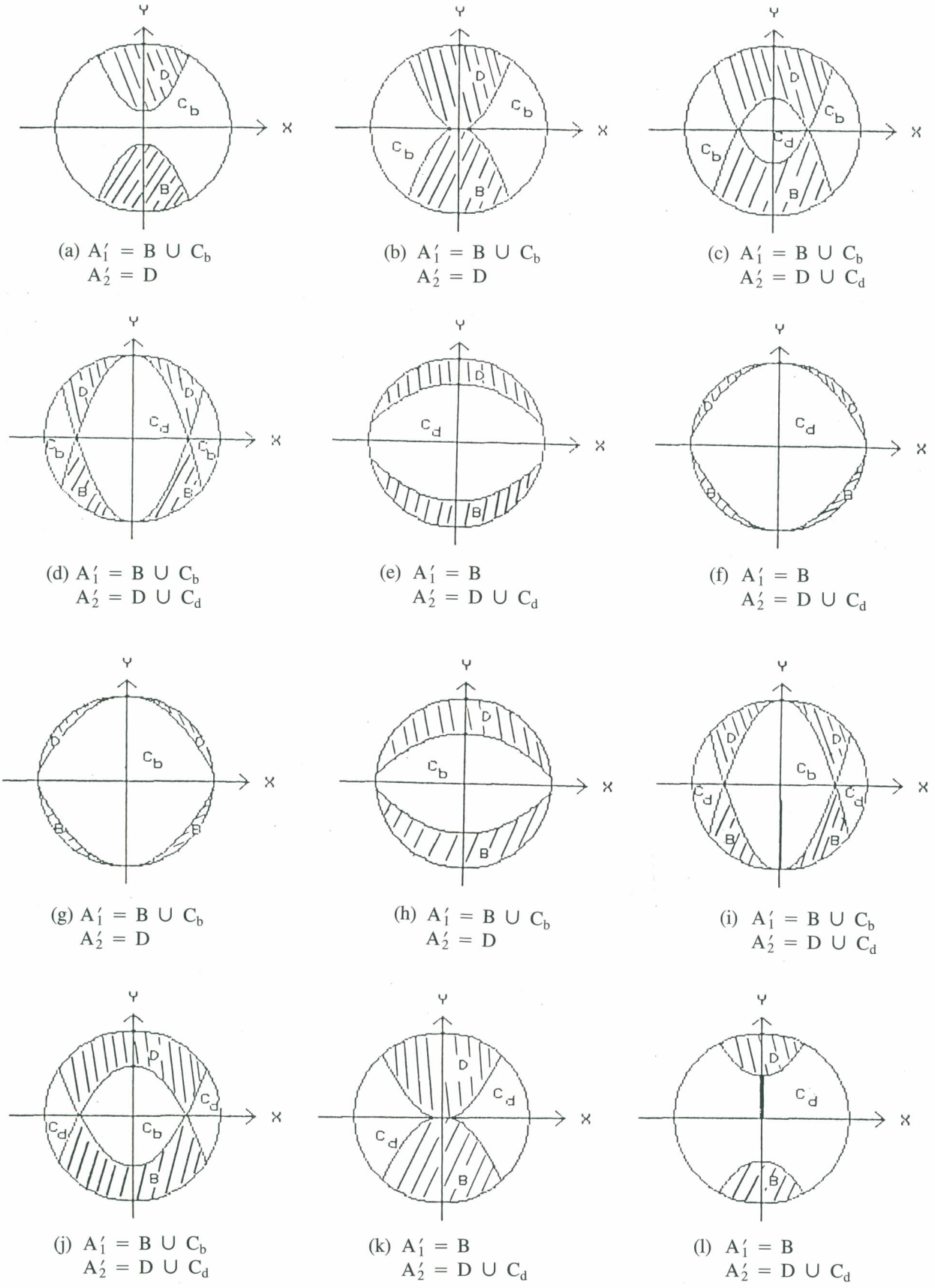

(a) $A_1' = B \cup C_b$, $A_2' = D$ (b) $A_1' = B \cup C_b$, $A_2' = D$ (c) $A_1' = B \cup C_b$, $A_2' = D \cup C_d$

(d) $A_1' = B \cup C_b$, $A_2' = D \cup C_d$ (e) $A_1' = B$, $A_2' = D \cup C_d$ (f) $A_1' = B$, $A_2' = D \cup C_d$

(g) $A_1' = B \cup C_b$, $A_2' = D$ (h) $A_1' = B \cup C_b$, $A_2' = D$ (i) $A_1' = B \cup C_b$, $A_2' = D \cup C_d$

(j) $A_1' = B \cup C_b$, $A_2' = D \cup C_d$ (k) $A_1' = B$, $A_2' = D \cup C_d$ (l) $A_1' = B$, $A_2' = D \cup C_d$

Fig. 4. The circle in each case of fig. 3 is divided into three or four parts B, D, C_b, and C_d. B is symmetric of D about the X-axis, and C_b and C_d both are symmetric to themselves about the X-axis.

$$+ \frac{h_2 \left(\int_D\int y'dx'dy' + \int_{C_d}\int y'dx'dy'\right)}{h_1 \int_{A_1'}\int dx'dy' + h_2 \int_{A_2'}\int dx'dy'} .$$

Since both C_d and C_b are symmetric to themselves about the X-axis, the integration values over C_d or C_b in the above equation is zero. So, the above equation can be simplified to be

$$\bar{y}' = \frac{h_1 \int_B\int y'dx'dy' + h_2 \int_D\int y'dx'dy'}{h_1 \int_{A_1'}\int dx'dy' + h_2 \int_{A_2'}\int dx'dy'}$$

which can further be reduced to be

$$\bar{y}' = \frac{(h_2 - h_1) \int_D\int y'dx'dy'}{h_1 \int_{A_1'}\int dx'dy' + h_2 \int_{A_2'}\int dx'dy'}$$

because B is symmetric to D about the X-axis. Since $h_2 > h_1$ and the area of D is not zero, we get $\bar{y}' > 0$ and the theorem is proved.

By Theorem 1, we know that the point with coordinates $(\bar{x}',\bar{y}')$ is on the Y-axis which is the symmetrical axis of the rotated parabola. Hence, $(\bar{x},\bar{y})$ is on the symmetrical axis. By this result, we have the following corollary whose proof is easy and is omitted.

COROLLARY The angle q between the symmetrical axis of the original parabola and the X-axis satisfies the equations

$$cosq = \frac{\bar{x}}{\sqrt{\bar{x}^2 + \bar{y}^2}} , \tag{7}$$

$$sinq = \frac{\bar{y}}{\sqrt{\bar{x}^2 + \bar{y}^2}} . \tag{8}$$

Let the grids of the 4.5-unit circle be indexed as shown in Fig. 5. Then $(\bar{x},\bar{y})$ used in Eqs. (7) and (8) above can be calculated as follows:

$$\bar{x} = \frac{\sum_{j=1}^{k} x_j I_j W_j}{\sum_{j=1}^{k} I_j W_j} , \tag{9}$$

$$\bar{y} = \frac{\sum_{j=1}^{k} y_j I_j W_j}{\sum_{j=1}^{k} I_j W_j} , \tag{10}$$

where

I_j = the intensity associated with the jth grid,
W_j = the weight associated with the jth grid,
(x_j,y_j) = the coordinates of the center of the jth gird, and
k = 69.

		1	2	3	4	5		
	6	7	8	9	10	11	12	
13	14	15	16	17	18	19	20	21
22	23	24	25	26	27	28	29	30
31	32	33	34	35	36	37	38	39
40	41	42	43	44	45	46	47	48
49	50	51	52	53	54	55	56	57
	58	59	60	61	62	63	64	
		65	66	67	68	69		

Fig. 5. Indexing associated with each square grid.

Following Tabatabai and Mitchell [16], we take W_j to be the fraction of the intersection area of the jth grid and the disk enclosed by the circle. This leads to the following W_j values:

W_j = .0084670539, j = 1,5,13,21,49,57,65,69;
= .013782918, j = 2,4,22,30,40,48,66,68;
= .013068037, j = 6,12,58,64;
= .01557318963, j = 3,31,39,67;
= .015719006, otherwise.

Now, we have completed the derivation of Eqs. (7) and (8) for calculating the q parameter. It remains to solve the other two parameters a and b.

DERIVATIONS OF THE EQUATIONS FOR COMPUTING THE *a* AND *b* PARAMETERS

Let D denote the set of the grids enclosed in the 4.5-unit circle C defined previously. Define the first three sample moments of the empirically obtained data in circle C as

$$m_i = \sum_{j=1}^{k} W_j I_j^i \qquad i = 1, 2, 3 .$$

By preserving the first three moments in the output of the detector, we get the following three equalities:

$$p_1h_1 + p_2h_2 = m_1 ,$$

$$p_1h_1^2 + p_2h_2^2 = m_2 ,$$

$$p_1h_1^3 + p_2h_2^3 = m_3 ,$$

where the three left terms of the above equations are the first three moments of the output data in disk C, and the fractions p_1 and p_2 are

$$p_1 = a_1 / \pi R^2 ,$$

$$p_2 = 1 - p_1 = a_2 / \pi R^2$$

where $R = 4.5$. Note that a_1 and a_2 are the areas of A_1 and A_2, respectively. Now, we can solve the above equations to obtain p_1, p_2, h_1, and h_2 as follows [16]:

$$h_1 = m_1 - d\sqrt{p_2 / p_1} ,$$

$$h_2 = m_1 + d\sqrt{p_1 / p_2} ,$$

$$p_1 = (1/2)\,[\,1 + s\sqrt{1 / (4 + s \times s)}\,] ,$$

where

$$s = (m_3 + 2m_1^3 - 3m_1m_2) / d^3 ,$$

$$d^2 = m_2 - m_1^2 .$$

Therefore, a_1 and a_2 can be computed by $a_1 = p_1 \pi R^2$ and $a_2 = p_2 \pi R^2$, respectively.

Rotating circle C counterclockwise with respect to the origin through an angle of $\pi/2 - q$, we can get the rotated parabola as shown in Fig. 3. In the following, we only investigate case (a) of Fig. 3; the other cases can be similarly treated. Let the rotated parabola with equation $ax^2 + b = y$ intersect the circle at two points (x_0, y_0) and $(-x_0, y_0)$ as indicated in Fig. 6. The shaded area, a_2, of the pattern is given by

$$a_2 = \int_{-x_0}^{x_0} \int_{ax^2+b}^{y_0} dydx + (\pi/2 - \beta)R^2 - x_0y_0$$

$$= x_0y_0 - 2ax_0^3/3 - 2bx_0 + (\pi/2 - \beta)R^2 .$$

Since $cos^{-1}(y_0/R) = \pi/2 - \beta$, $0 \le cos^{-1}(y_0/R) \le \pi$, it follows that

$$x_0y_0 - 2ax_0^3/3 - 2bx_0 + R^2 cos^{-1}(y_0/R) = a_2 , \tag{11}$$

where (x_0, y_0) satisfies the following two equations:

$$x_0^2 + y_0^2 = R^2 , \tag{12}$$

$$ax_0^2 + b = y_0 . \tag{13}$$

THEOREM 2 The following equality is true:

$$r = \frac{(h_2 - h_1)(x_0R^2 - x_0^3/3 - a^2x_0^5/5 - 2abx_0^3/3 - b^2x_0)}{h_1a_1 + h_2a_2} , \tag{14}$$

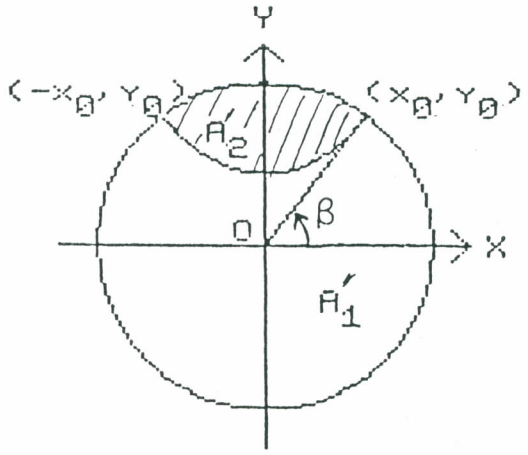

Fig. 6. A rotated parabola intersecting the circle at two points (x_0,y_0) and $(-x_0,y_0)$.

where $r = \sqrt{\bar{x}^2 + \bar{y}^2}$ is the distance from the origin to the original center of gravity.

Proof By Theorem 1,

$$r = \sqrt{\bar{x}^2 + \bar{y}^2}$$

$$= \sqrt{\bar{x}'^2 + \bar{y}'^2}$$

$$= \bar{y}' . \tag{15}$$

Combining Eqs. (6) and (15), we have

$$r = \frac{h_1 \int_{A_1'} \int y'dx'dy' + h_2 \int_{A_2'} \int y'dx'dy'}{h_1 \int_{A_1'} \int dx'dy' + h_2 \int_{A_2'} \int dx'dy'} ,$$

which can be simplified, according to Fig. 3a, to be

$$r =$$

$$[\, h_1 (\int_{-R}^{-x_0} \int_{-\sqrt{R^2-x^2}}^{\sqrt{R^2-x^2}} ydydx + \int_{-x_0}^{x_0} \int_{-\sqrt{R^2-x^2}}^{ax^2+b} ydydx$$

$$+ \int_{x_0}^{R} \int_{-\sqrt{R^2-x^2}}^{\sqrt{R^2-x^2}} ydydx) + h_2 \int_{-x_0}^{x_0} \int_{ax^2+b}^{\sqrt{R^2-x^2}} ydydx\,]$$

$$/ (h_1a_1 + h_2a_2)$$

$$= \frac{(h_2 - h_1)(x_0R^2 - x_0^3/3 - a^2x_0^5/5 - 2abx_0^3/3 - b^2x_0)}{h_1a_1 + h_2a_2} .$$

And the theorem is proved.

Now, solving Eqs. (12) and (13) to obtain x_0 and y_0 in terms of a and b and substituting the results into Eqs. (11) and (14), we can obtain two nonlinear equations with two unknown parameters a and b. A numerical

method must be used to get the solutions. For this, Newton's method [5] is used.

For the method to result in accurate solutions, we must start with good initial values (a_0, b_0) that are near the desired solutions. Since a curved edge in a 4.5-unit circle is nearly linear, a is close to zero. For safety, we enumerate a_0 from 0 to ± 3 with step increments of 0.2 or -0.2 alternatively (i.e., $a_0 = 0, 0.2, -0.2, 0.4, -0.4, \ldots$) until the solutions are found. Also, we know that $-4.5 < b < 4.5$, so we enumerate b_0 from -4 to 4 with step increments of 0.5 until the solutions are found. Now, all three parameters a, b, and q have been solved, by which we can compute curved edge locations to subpixel values.

If we set $a = 0$, it can be shown that the curved edge detector becomes the Tabatabai-Mitchell line edge detector [16]. This means that the proposed detector can detect line edges. Figs. 7, 8, and 9 show the results obtained by applying the proposed detector to several empirical input edge patterns. For the sake of comparison, the Tabatabai-Mitchell edge detector is also applied to the same input patterns. Fig. 7 shows that the proposed edge detector has the similar capability as the Tabatabai-Mitchell detector in line-type edge detection. Figs. 8 and 9 show that the proposed detector is better than the Tabatabai-Mitchell detector when the edge occurs at a corner or on a curved boundary.

EXPERIMENTAL RESULTS

To apply the proposed detector, a digital image of size 256 × 240 is first divided into a set of contiguous overlapping 4.5-unit circles as shown in Fig. 10. The distance between the centers of every two neighboring circles in the horizontal (or vertical) direction is 5 pixels.

The curved edge detector is repeatedly applied to each circle. A curved edge pattern is determined to exist in a circle if the computed h_1 and h_2 values satisfy the following inequality [1]:

$$h_2 - h_1 \geq d \,. \tag{16}$$

This means that if an edge pattern is considered to exist between two neighboring regions in the circle, then one region must be "dark" enough with respect to the other. The value of d can be determined experimentally, but a more intelligent method is used here [1]. By considering the original image as a blurred noisy version of a binary input picture, the moment-preserving bilevel thresholding proposed by Tsai [17] is applied globally to the whole image to get two representative gray levels z_0 and z_1 (with $z_1 > z_0$). The value d is selected to be $(z_1 - z_0)/2$. If the original image cannot be regarded as a binary version, we can divide the image into smaller, nearly binary blocks and then locally apply the foregoing method to each block to get a distinct d value.

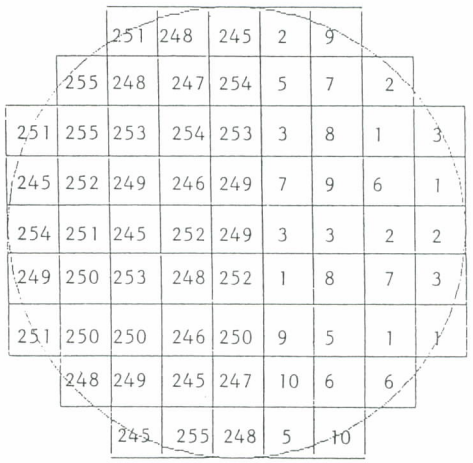

(a) Two-dimensional input edge pattern.

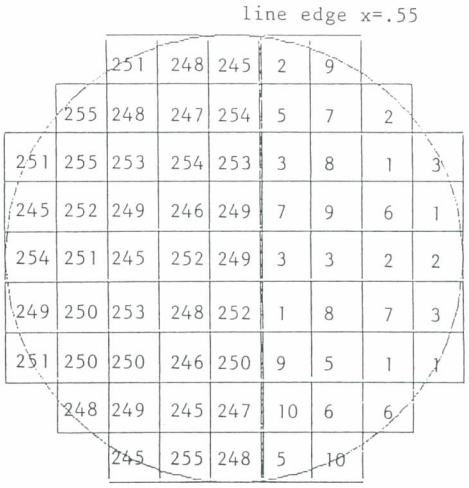

(b) Result of applying the proposed edge detector to (a) – a line equation x = .55.

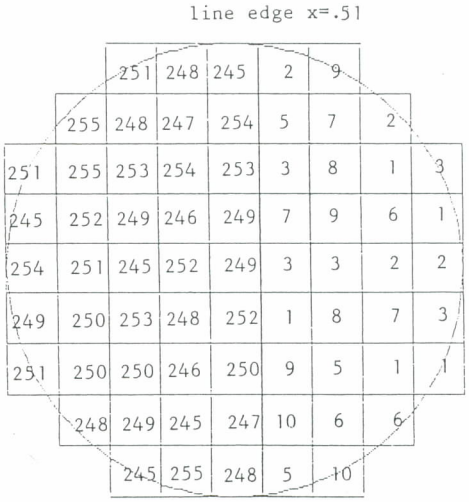

(c) Result of applying the Tabatabai-Mitchell edge detector to (a) – a line equation x = .51.

Fig. 7. Result of applying the proposed detector to line-type edges is similar to that of applying the Tabatabai-Mitchell detector.

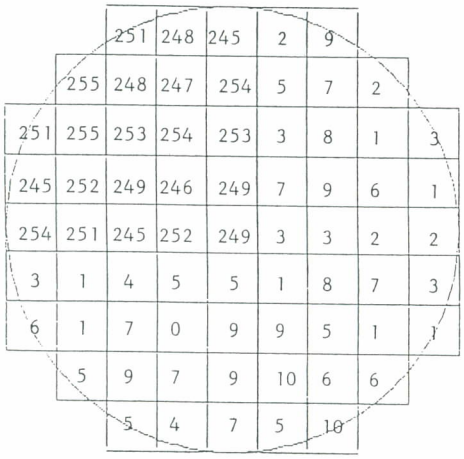

(a) Two-dimensional input edge pattern.

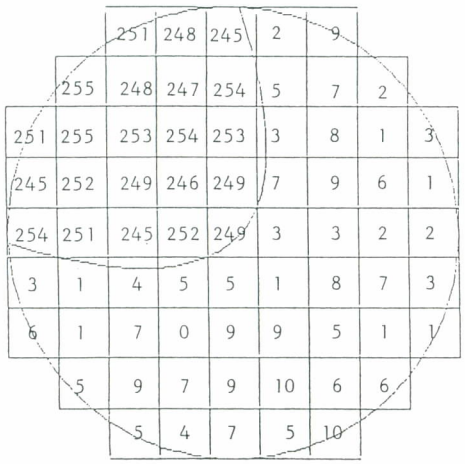

(b) Result of applying the proposed edge detector to (a) – a parabolic equation $0.29\ (0.7x+0.71y)^2 - 0.14 = -0.71x+0.7y$.

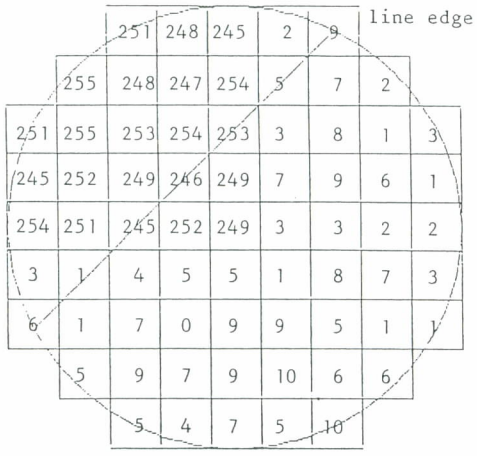

(c) Result of applying the Tabatabai-Mitchell edge detector to (a) – a line equation $-0.71x+0.7y = 1.38$.

Fig. 8. A better result of the proposed detector for corner finding than the Tabatabai-Mitchell detector.

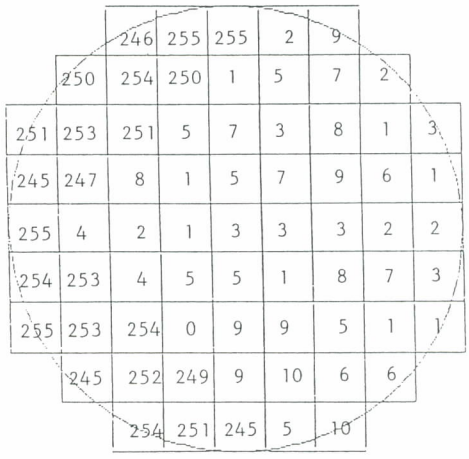

(a) Two-dimensional input edge pattern.

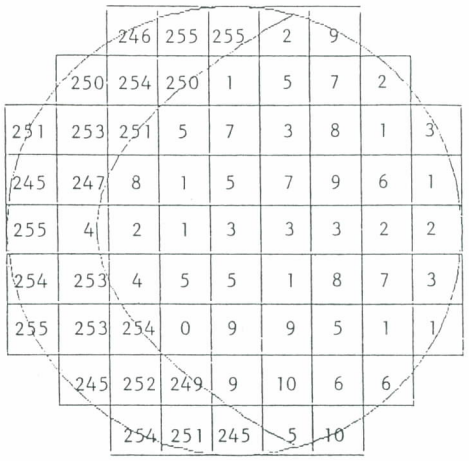

(b) Result of applying the proposed edge detector to (a) – a parabolic equation $x = 0.21y^2 - 2.74$.

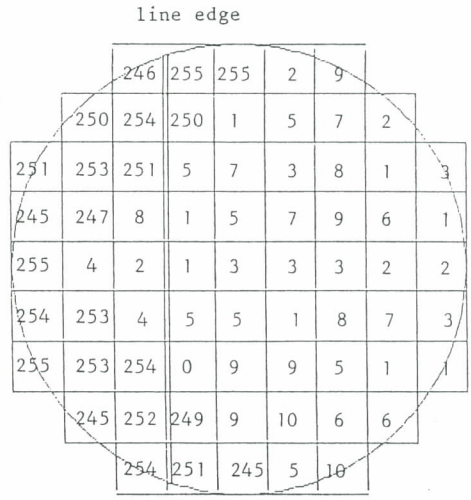

(c) Result of applying the Tabatabai-Mitchell edge detector to (a) – a line equation $x = -1.42$.

Fig. 9. A better result of the proposed detector for curved boundary detection than the Tâbatabai-Mitchell detector.

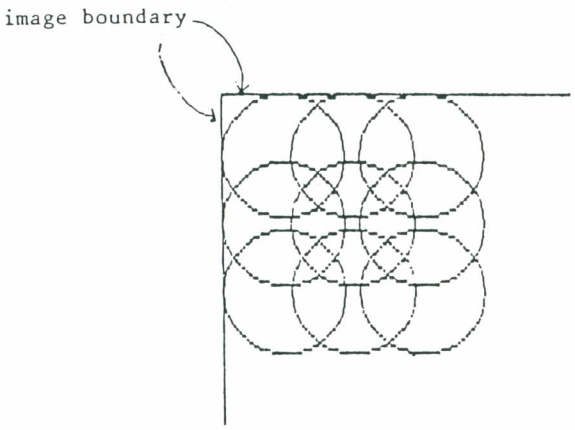

Fig. 10. The locations of the circles for the purpose of edge detection.

If Inequality (16) is not satisfied, we conclude that a curved edge pattern is not present. Otherwise, we test further for the condition [1]:

$$\frac{h'_2 - h'_1}{h_2 - h_1} \geq \delta \ ; \tag{17}$$

where

$$h'_1 = (1/a_1) \int_{A_1}\int I(x,y)\ dxdy$$

is the mean of the observed intensity values in area A_1;

$$h'_2 = (1/a_2) \int_{A_2}\int I(x,y)\ dxdy$$

is the mean of the observed intensity values in area A_2; and $I(x,y)$ is the observed intensity value at location (x,y) which is constant over the grid centered at (x,y). This step is employed to avoid considering as a parabolic pattern a curved edge pattern which is not close to a parabola or which is just noise existing in the detection circle. The selection of the threshold value δ depends on the requirement for the accuracy of the detected curved edges. In our experiment we set δ to be 0.87. If both (16) and (17) are satisfied, then we conclude that a well-shaped parabolic edge pattern is present in the input circles, and

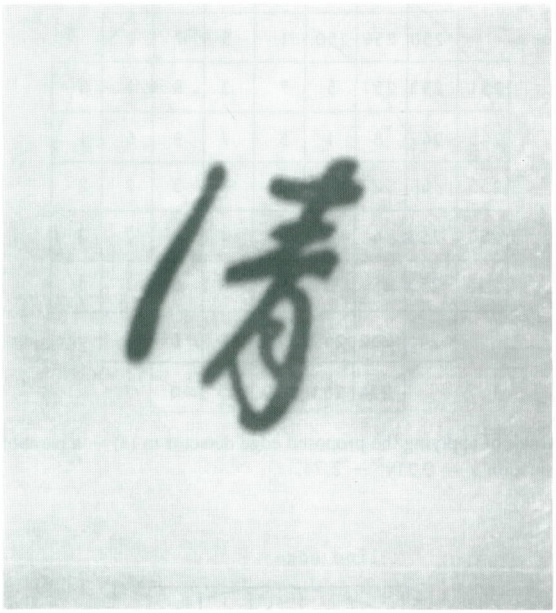

(a) Original input image.

(b) Output image with detected parabolas drawn in each detected circle area.

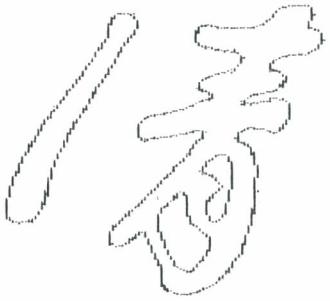

(c) Output image resulting from detection identical to that of (b) except that the curved edge detection is additionally applied to some of 24 neighboring points of origin of each detection circle in (b) in which curved edge pattern is not detected.

(d) Result of Tabatabai-Mitchell edge detector.

Fig. 11. Results of applying various edge detectors to a character image.

generate the parabolic pattern as the output.

Figure 11a includes a Chinese character with many curved edges and sharp turns. Fig. 12a includes a toy with smooth edges. Figs. 11b and 12b show the results of the curved edge detector. In every circle of each output image, the detected parabola is drawn according to its equation. From the output images we see that certain curved edges are missing. The reasons for this include the following: (1) the missing curved edges are not close to parabolas; (2) the symmetrical axis of the parabola does not pass through the center of the detection circle. To avoid these situations, a method proposed by Chen and Tsai [1] is employed here. In each of such detection circles, a 5×5 neighborhood of the origin is taken. Then we order the pixels in the 5×5 neighborhood by their Euclidean distances to the origin as follows.

22	15	10	14	21
16	6	2	5	13
11	3	0	1	9
17	7	4	8	20
23	18	12	19	24

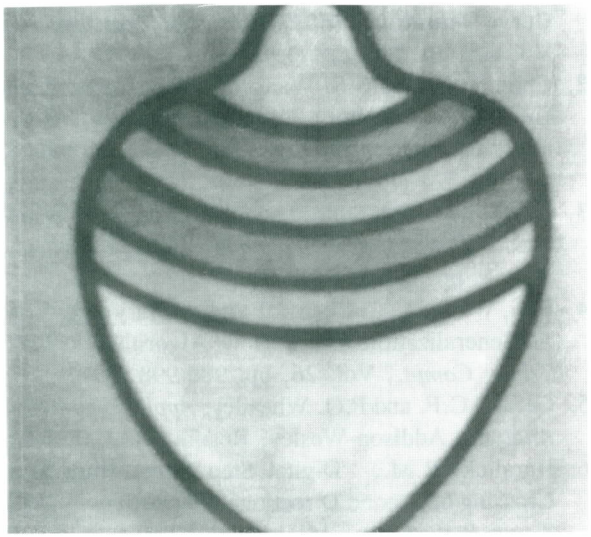

(a) Original input image.

(b) Output image with detected parabolas drawn in each detected circle area.

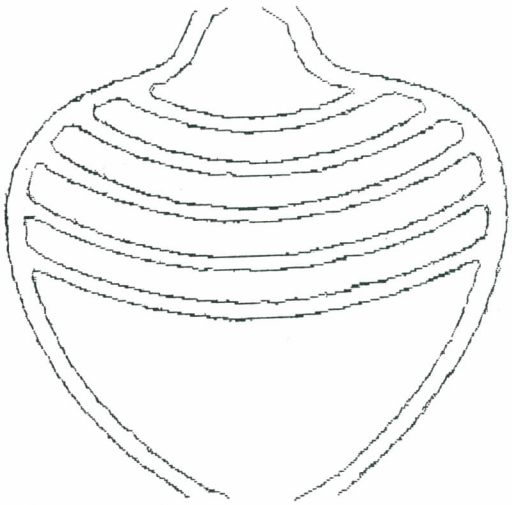

(c) Output image resulting from detection identical to that of (b) except that the curved edge detection is additionally applied to some of 24 neighboring points of origin of each detection circle in (b) in which curved edge pattern is not detected.

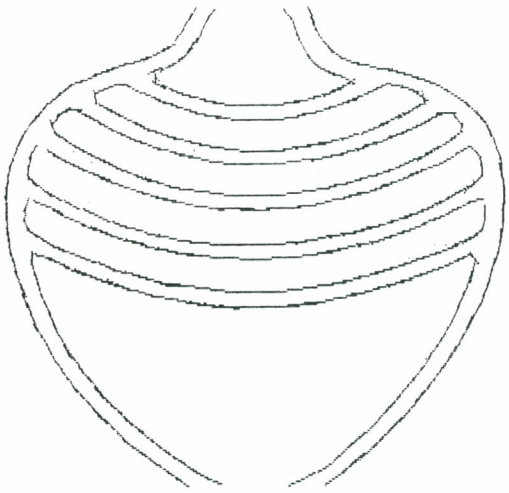

(d) Result of Tabatabai-Mitchell edge detector.

Fig. 12. Results of applying various edge detectors to a toy image.

According to the order, pixels in the neighborhood are taken in turn, and the proposed curved edge detection procedure is applied iteratively to the 4.5-unit circle with each pixel as the center until an acceptable solution is found or until all pixels have been processed. If an acceptable parabolic pattern exists, then we take it as the output of the original detection circle. Applying this method to Figs. 11a and 12a, we have the results as shown in Figs. 11c and 12c. All curved edges in each image have been detected. It is seen that the proposed detector gives good results for curvilinear edges, including line edges, smooth curved edges, corner edges, and unsmooth curved edges. Figs. 11d and 12d show the results of the Tabatabai-Mitchell detector. Obviously, the line edge detector flattens certain curved edges and does not give proper approximations at corner edges. On the contrary, the proposed curved edge detector gives better results.

CONCLUSIONS

A new curved edge detector has been proposed, which can locate a step edge to subpixel accuracy in two-dimensional image data. Using parabolas to approximate edge points, the method gives better results of curved edge location than conventional line edge detectors. If a parameter of the parabola equation is restricted to be 0, the proposed detector becomes equivalent to the Tabatabai-Mitchell detector.

If the curved edge in a detection area is not close to a parabola, then the proposed detector is not applicable. Therefore, using curved-type equations other than the parabola to approximate curved edges is also worth trying.

NOMENCLATURE

(a,b,q)	the three parameters of a parabola
a_1	the area of A_1
a_2	the area of A_2
A_1	a region in a circle
A_2	a region in a circle
A_1'	the rotation version of A_1
A_2'	the rotation version of A_2
d	a threshold value
h_1	the intensity value in region A_1
h_2	the intensity value in region A_2
I_j	the intensity associated with the jth grid
K	the pixel number in a circle
m_i	the ith sample moment of the empirically obtained data in a circle
p_1	the fraction of A_1 in a circle
p_2	the fraction of A_2 in a circle
R	the radius of a circle
r	the distance from the origin to the original center of gravity
(x,y)	the coordinates of a point in the original parabola
(x',y')	the new coordinates of the point (x,y) in the rotated parabola
$(\bar{x},\bar{y})$	the coordinates of the center of gravity of the intensities of the output data inside a circle
$(\bar{x}',\bar{y}')$	the coordinates of the center of gravity of the intensities inside the rotated circle
(x_j,y_j)	the coordinates of the center of the jth grid
W_j	the weight associated with the jth grid

Greek symbol

δ	a threshold value

REFERENCES

1. Chen, L.H. and W.H. Tsai, "Moment-Preserving Curve Detection," *IEEE Trans. Syst. Man Cybern.*, Vol. 18, pp. 148-158 (1988).
2. Chen, L.H. and S.S. Wang, "A Two-Layer Area-Level Edge Detector – A New Approach," *Journal of Information Science and Engineering*, Vol. 6, pp. 311-324 (1990).
3. Davis, L.S., "A Survey of Edge Detection Techniques," *Comput. Vision, Graphics, Image Process.*, Vol. 4, pp. 248-270 (1975).
4. Frei, W. and C.C. Chen, "Fast Boundary Detection: A Generalization and a New Algorithm," *IEEE Trans. Compt.*, Vol. 26, pp. 988-998 (1977).
5. Gerald, C.F. and P.O. Wheatley, *Applied Numerical Analysis*, Addison-Wesley, Reading, MA (1983).
6. Haralick, R.M., "Digital Step Edges from Zero Crossing of Second Directional Derivatives," *IEEE Trans. Pattern Anal. Mach. Intell.*, Vol. 6, pp. 58-68 (1984).
7. Hartley, R., "A Gaussian-Weighted Multiresolution Edge Detector," *Compt. Vision, Gaphics, Image Process.*, Vol. 30, pp. 70-83 (1985).
8. Hueckel, M.H., "An Operator Which Locates Edges in Digitized Pictures," *J. Assoc. Comput. Mach.*, Vol. 18, pp. 113-125 (1971).
9. Hyde, P.D. and L.S. Davis, "Subpixel Edge Estimation," *Pattern Recognit.*, Vol. 16, No. 4, pp. 413-420 (1983).
10. Jacobus, C.J. and R.T. Chien, "Two New Edge Detectors," *IEEE Trans. Pattern Anal. Mach. Intell.*, Vol. 3, pp. 581-592 (1981).
11. Rosenfeld, A. and A.C. Kak, *Digital Picture Processing*, Vol. 2, Academic Press, New York (1982).
12. Schachter, B.J. and A. Rosenfeld, "Some New Methods of Detecting Step Edges in Digital Pictures," *Commun. Assoc. Compt. Mach.*, Vol. 21, pp. 172-176 (1978).
13. Shipman, A.L., R.R. Bitmead and G.H. Allen, "Diffuse Edge Fitting and Following: A Location-Adaptive Approach," *IEEE Trans. Pattern Anal. Mach. Intell.*, Vol. 6, pp. 96-102 (1984).
14. Suk, M. and S. Hong, "An Edge Extraction Techni-

que for Noisy Images,'' *Compt. Vision, Graphics, Image Process.*, Vol. 25, pp. 24-45 (1984).
15. Synge, J.L. and B.A. Griffith, *Principles of Mechanics,* McGraw-Hill, New York, pp. 75-76 (1949).
16. Tabatabai, A.J. and O.R. Mitchell, ''Edge Location to Subpixel Values in Digital Imagery,'' *IEEE Trans. Pattern Anal. Mach. Intell.*, Vol. 6, pp. 188-201 (1984).
17. Tsai, W.H., ''Moment-Preserving Thresholding: A New Approach,'' *Comput. Vision, Graphics, Image Process.*, Vol. 29, pp. 377-393 (1985).

Discussions of this paper may appear in the discussion section of a future issue. All discussions should be submitted to the Editor-in-Chief.

Manuscript Received: July 3, 1991
Revision Received: March 4, 1992
and Accepted: Aug. 19, 1992